



ELSEVIER

20 May 2002

Physics Letters A 297 (2002) 396–401

PHYSICS LETTERS A

www.elsevier.com/locate/pla

Noise-induced effects on the chaotic advection of fluid flow

J.P. Baltanás^a, A. Zaikin^b, F. Feudel^b, J. Kurths^b, M.A.F. Sanjuán^{a,*}

^a *Nonlinear Dynamics and Chaos Group, Universidad Rey Juan Carlos, Tulipán s/n, 28933 Móstoles, Madrid, Spain*

^b *Institute of Physics, University of Potsdam, Am Neuen Palais 10, 14469 Potsdam, Germany*

Received 18 December 2001; received in revised form 22 March 2002; accepted 22 March 2002

Communicated by C.R. Doering

Abstract

This Letter analyzes the role played by harmonic noise on the chaotic advection of passive tracers of a fluid flow model in order to show that noise is able to recover intrinsic dynamical properties of some nonlinear systems. Stroboscopic maps of the fluid flow are analyzed by using an appropriate time-periodic stream function, deterministic versus stochastic, and a method consisting in the computation of a probability density. We show that under certain conditions the noise-induced behavior closely resembles the effect of a deterministic time-periodic external perturbation, including the appearance of KAM tori. © 2002 Published by Elsevier Science B.V.

The study of nonlinear phenomena has constituted one of the principal topics of research in the past few years. A special role has been played by the counter-intuitive ability of noise to induce order in nonlinear nonequilibrium systems. In fact, the randomness of the environment of an open nonequilibrium dynamical system, which has been considered in the past only as a nuisance, may be used now for positive purposes. Perhaps the best example of such a noise-induced phenomenon is stochastic resonance [1,2], although other important effects of noise in nonlinear dynamical systems such as noise-induced transitions [3–5], stochastic transport in ratchets [6], coherence resonance [7] and noise-induced pattern formation [8] might be cited as well.

Another interesting aspect of these studies is the ability of noise to excite a dynamical behavior in the nonlinear system which closely resembles its behavior in a deterministic case. This effect is a manifestation of the fact that under certain conditions noise is able to recover intrinsic dynamical properties of the nonlinear system. In this case an external noisy perturbation excites only natural motions of the system. Hence, surprisingly, despite the random character of the excitation, the behavior of the system looks like the motion excited by a harmonic external force [9] or a self-excitation mechanism [10]. In many cases the distinction between noise-induced stochastic oscillations and deterministic behavior is rather difficult to establish and requires special methods of analysis [5].

Following this idea, our goal here is to analyze the influence of noise on the chaotic advection of passive tracers of a fluid flow, where an external deterministic forcing is applied. The phenomenon of chaotic advection has attracted the interest of many

* Corresponding author.

E-mail address: msanjuan@escet.urjc.es (M.A.F. Sanjuán).

researchers (see, for instance [11,12]), where time-periodic two-dimensional fluid flows have been used. This is precisely the case in which we are interested. We review shortly the model introduced in [13,14] before the results of our numerical simulations are outlined and discussed.

The influence of noise is studied on a simple fluid model which originates from experiments which are described in Refs. [15–18] and by numerical investigations of the two-dimensional Navier–Stokes equations in [19–21]. Instabilities and transitions in a linear chain of electrically driven vortices were studied in these experiments and could be recovered by computations of the externally forced two-dimensional Navier–Stokes equations. Numerical simulations gave strong evidence that the essential dynamics, at least for moderate Reynolds numbers, may be described by a low-dimensional, five-mode, stream function model [13]. This five-mode approximation was analyzed by Witt et al. in Ref. [14] in order to study the chaotic advection of passive tracer particles injected into the fluid. An external deterministic time-periodic perturbation on the stream function was applied in order to simulate the dynamics of the flow beyond the Hopf bifurcation in the case that the Reynolds number exceeded a critical value. This time-periodic flow consists of a series of corotating vortices and a shear component. But the dynamics of the passive tracers has got already a chaotic nature in a thin layer which separates the vortices from the shear flow. The main result was to show the existence of a chaotic saddle (also called nonattracting chaotic set) which is believed to be the responsible of the tracer dynamics in this chaotic layer. In fact, the transient chaos which is present in the dynamics of the fluid flow, is a consequence of this nonattracting chaotic set, which is composed by the intersection of the unstable and the stable manifolds of a fixed point in the phase space.

For our purposes and in order to keep the essential properties of the flow studied in [14], we make a further simplification and retain only the two more important modes in the stream function model. The stream function is given then by

$$\psi(x, y) = \psi_{01} \sin(y) + \psi_{21} \sin(2x) \sin(y), \quad (1)$$

where ψ_{01} measures the strength of the shear flow and ψ_{21} represents the flow component of the driven vorticity. Moreover, it shows qualitatively a good agree-

ment with the dynamics resulting from the Navier–Stokes computations in [21] and reflects essential features of the experiments we have mentioned above.

For a stationary flow the pathlines of the tracers coincide with the streamlines and provide a direct visualization of the velocity field. In the time-dependent regime, which is the one we are interested, the situation is more complicated and the pathlines have to be determined by the integration of the nonautonomous equations of motion of the velocity field of the fluid flow which are given by

$$\dot{x} = \frac{\partial \psi(\mathbf{x}, t)}{\partial y}, \quad \dot{y} = -\frac{\partial \psi(\mathbf{x}, t)}{\partial x}, \quad (2)$$

where $\mathbf{x} = (x, y)$ represent the coordinates of the points in the two-dimensional phase space of the tracer particle. Note that these equations are simply Hamilton's equations, since the stream function $\psi(\mathbf{x}, t)$ might be viewed as a Hamiltonian function. Moreover for time-dependent periodic flows the pathlines show a very complicated, wrinkled, and chaotic form, a phenomenon also known as Lagrangian chaos or Lagrangian turbulence.

Matching the investigations in [14], we introduce a particular time-dependence of the flow varying only the coefficient ψ_{01} . This model also reflects the dynamics of the flow of driven vortices which results from the Navier–Stokes simulations performed in [13, 21]. For the deterministic situation we modulate ψ_{01} as

$$\psi_{01}(t) = \psi_{01} [1 + \mu \sin(\omega_0 t)], \quad (3)$$

where μ is a constant and measures the strength of the harmonic excitation. Specifying the coefficients $\psi_{01} = 8.35$ and $\psi_{21} = -2.55$ as in [14], the resulting flow reproduces qualitatively the same streamlines as the Navier–Stokes flow described in [13,21].

For the visualization of the dynamics of externally driven systems, we use the standard technique of stroboscopic maps. The trajectories are mapped on the Poincaré section by sampling them at multiple times of the driving period. A stroboscopic map for a set of tracers driven by the pure deterministic forcing is shown in Fig. 1, which is in accordance to Eq. (3) and governed by Eq. (2). The dynamics of the fluid flow is analyzed in the spatial domain $\Omega = [0, \pi] \times [0, \pi]$, once we have taken into account symmetry considerations of the stream function. The

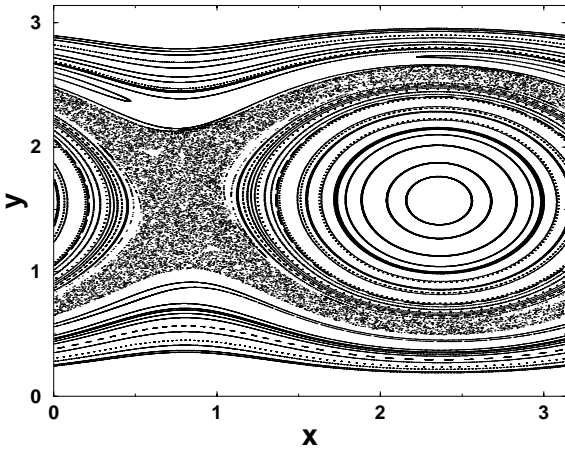


Fig. 1. Stroboscopic map for a set of tracer particles in the pure deterministic situation for $\omega_0 = \pi$ and $\mu = 0.2$ according to Eq. (3).

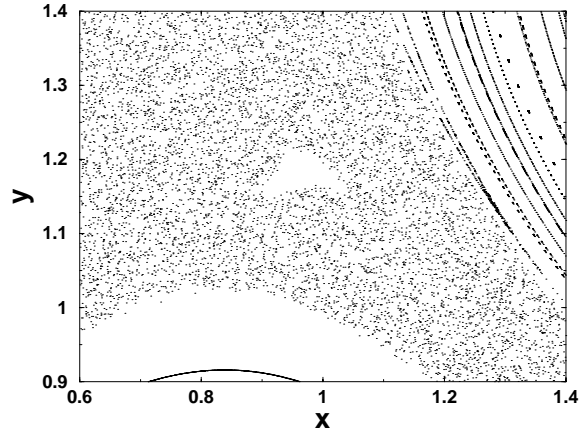


Fig. 2. Blow-up of the stochastic layer around the lower KAM torus of Fig. 1.

flow consists of one vortex in the middle and a shear flow on top and bottom that are separated by a chaotic layer. The regular tracer motion near the center of the vortex and in the shear region is mirrored by smooth lines. Due to the Hamiltonian structure of Eq. (2), that are periodically perturbed by Eq. (3), one expects surviving KAM tori. The layer is interspersed by infinitely many KAM tori, but only the largest of them are discernible. In Fig. 2 a blow-up of the chaotic region appears, where one of these typical KAM tori is shown in detail, in order to make it clear the appearance of these surviving structures in the stochastic layer.

The aim of this Letter is to study the effect of noise on the system governed by the stream function in Eq. (1) when we replace the deterministic time-dependent term in Eq. (3) by a stochastic excitation

$$\psi_{01}(t) = \psi_{01}[1 + \chi(t)]. \tag{4}$$

The $\chi(t)$ used here is the so-called *harmonic noise* which is described by the stochastic differential equation

$$\ddot{\chi}(t) + 2\delta\dot{\chi}(t) + \omega_0^2\chi(t) = \xi(t), \tag{5}$$

where $\xi(t)$ is a zero mean, Gaussian white noise with a time correlation function given by

$$\langle \xi(t)\xi(t') \rangle = \Delta\delta(t - t'). \tag{6}$$

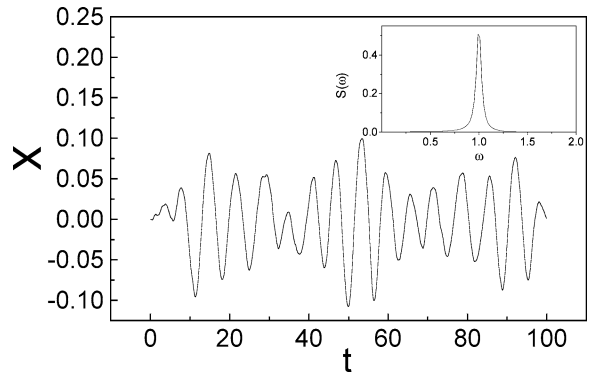


Fig. 3. A sample realization of harmonic noise for $\omega_0 = 1$, $\delta = 0.03$ and $\Delta = 0.0002$. In the inset, the spectral power density of the noise for this set of parameters is plotted.

The spectral density of the process $\chi(t)$ is then

$$S(\omega) = \frac{\Delta}{(\omega^2 - \omega_0^2)^2 + 4\delta^2\omega^2}. \tag{7}$$

A realization of harmonic noise for the parameter values $\omega_0 = 1$, $\delta = 0.03$ and $\Delta = 0.0002$ is plotted in Fig. 3. The important point is that despite its short temporal span, this realization clearly shows both the stochastic oscillatory component and the slower random modulation in amplitude. In the inset, a plot of the spectral density of the noise, $S(\omega)$, for the same set of parameters is depicted. It is straightforward to obtain from Eq. (7) that the maximum value for $S(\omega)$

reads

$$S(\omega_{\max}) = \frac{\Delta}{4\delta^2\omega_0^2(1 - (\delta^2/\omega_0^2))}, \tag{8}$$

which can be considered as the harmonic noise intensity.

The role of the damping parameter δ on the behavior of the system is considered first, focusing our attention in the analysis of the fluid flow by the use of the stroboscopic maps. In our case, where the system is driven by a stochastic signal, the role of the driving period is played by $T_0 = 2\pi/\omega_0$, where ω_0 is the mean frequency of the harmonic noise (see Eq. (5)). Four stroboscopic maps corresponding to different values of δ are depicted in Fig. 4. We have fixed $\omega_0 = \pi$ for all cases, whereas Δ changes in order to keep constant the value of $S(\omega_{\max})$ as δ varies. This is done in order to assure that the obtained results are dependent only on the bandwidth and independent of the noise intensity. In particular, we have fixed $S(\omega_{\max})$ to the corresponding value for $\Delta = 0.001$, $\delta = 0.03$ and $\omega_0 = \pi$. For the smallest noise intensity $\delta = 0.0001$ (see Fig. 3(d)), the stroboscopic map resembles much the deterministic case, as shown in Fig. 1. Especially, some resemblances with the KAM tori that occur in the deterministic case can be seen here, although the

boundaries between the KAM tori and the rest of the stochastic layer are not so clear as in the deterministic case. As δ increases, features corresponding to the deterministic case tend to disappear, as it is seen in the previous three panels (Fig. 3(a)–(c)): KAM tori are not present in these cases and the stochastic layer and the shear part of the flow are less distinguishable as δ grows (see, for example, panel (a) which corresponds to $\delta = 0.1$). This is easily understood if we take into account that δ is related to the width of the peak of the harmonic noise spectrum (see Fig. 3), where the peak is wider as δ increases. This means that more frequencies contribute to the noise generation, i.e., the harmonic noise and the deterministic sine wave signal differ more as δ increases.

For a better description of the behavior of the system as δ varies the following approach is used. We have determined the location of the upper and lower KAM tori in the deterministic case, to be situated approximately at (0.61, 1.95) for the upper torus and at (0.95, 1.18) for the lower one. Then we define a narrow band parallel to the y axis that crosses the lower KAM torus and divide it in bins in order to compute the probability of having points of the stroboscopic map inside this band.

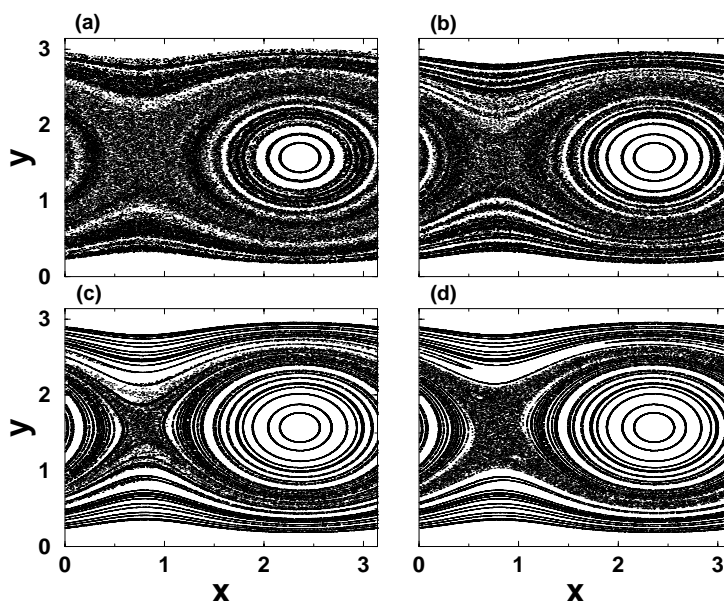


Fig. 4. Stroboscopic maps for the stochastic model, showing the behavior of the system when δ changes. In all cases $\omega_0 = \pi$ and $S(\omega_{\max})$ is a constant. The corresponding values of δ are (a) 0.1, (b) 0.01, (c) 0.001 and (d) 0.0001. Notice the presence of KAM tori for small δ .

The same procedure can be repeated with the upper KAM torus giving similar results. This probability density is expected to give an insight of how the stroboscopic map is modified when δ varies. We compute these histograms for different values of δ keeping $S(\omega_{\max})$ constant. One would expect the probability distribution to be almost constant for high values of δ along the line crossing the KAM torus, which would correspond to a rather homogeneous distribution of the points in the stroboscopic map. We have computed explicitly this probability distribution for a sufficiently high value of $\delta = 0.3$, with the result that no relevant structure is apparent, as expected (data not shown). On the other hand, some structures should appear in the histogram as δ decreases. This expectation is clearly confirmed in our simulations and is visible in Fig. 5(a),(b), where two histograms corresponding to $\delta = 0.01$ and $\delta = 0.0001$ are shown.

If we observe the histogram corresponding to $\delta = 0.0001$ (Fig. 4(b)); three zones are clearly discernible. In the approximate region of $0 < y < 1$ and $2.25 < y < \pi$, several sharp peaks appear which clearly correspond to the streamlines reflecting the shear part of the flow. Between these two similar regions, we find the part of the histogram which mirrors the stochastic layer from the stroboscopic map. In this zone we can distinguish the KAM torus location near $y = 1.18$, where the probability density drops to 0 abruptly. Around this value, large fluctuations in the probability distribution occur, whereas in the rest of this region the probability density is nearly a constant. We believe that they might give an indication for the creation of the KAM torus. In the other histogram for $\delta = 0.01$ (Fig. 5(a)), these structures are much less apparent or simply disappear. In particular, no evidence of the presence of a KAM torus can be seen from this histogram. We have also noticed that a change in the bin width used for the computation of the probability densities does not alter substantially our results.

As shown above, computations of the probability distributions can be a useful tool in describing the behavior of the system when a parameter is varied. Next, we apply this technique to the analysis of what, from our point of view, is a particularly interesting question. This consists on the differences and/or similarities between the stochastic and the deterministic cases, when the parameters for the harmonic noise are set to values such that the stroboscopic map for the stochastic

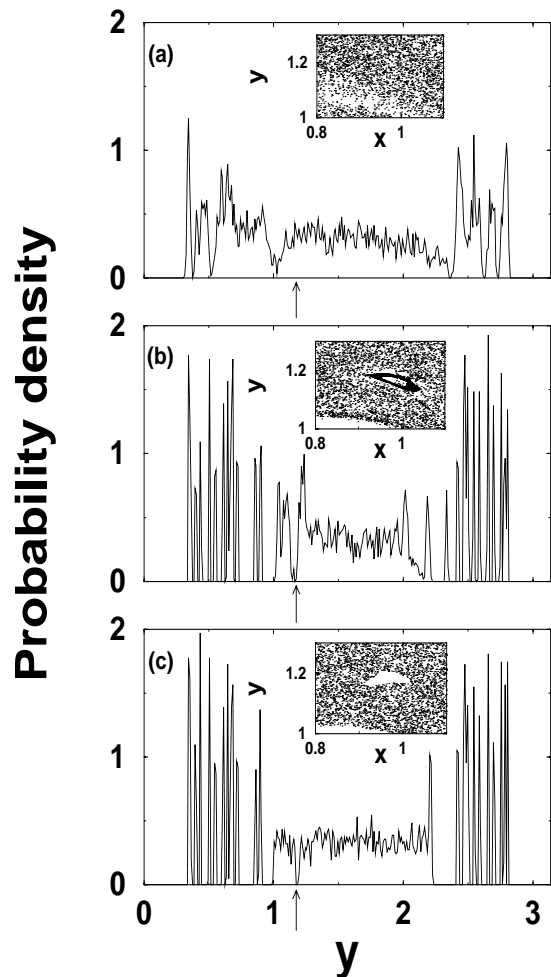


Fig. 5. (a) Histogram corresponding to the case of Fig. 3(b); (b) to the case of Fig. 3(d); (c) to the deterministic case of Fig. 1. The results correspond to the lower KAM tori ($x = 0.95$). Its y coordinate is shown by the arrow. Notice how the KAM torus location and fluctuations referred to in the text are clearly visible in (b). Note also the close similarity of the stochastic case (b) and the deterministic case (c). In the insets, large scaled regions showing the lower KAM tori location in all cases are depicted.

case is very similar to the deterministic one. We compare the case of the noisy excitation shown in the stroboscopic map of Fig. 4(d) with the deterministic case shown in Fig. 1. The corresponding probability density histograms are depicted in Fig. 4(b) and Fig. 4(c). It is clearly seen that, despite the fact that the system is driven by a purely stochastic term in Fig. 4(b) and by a deterministic signal in Fig. 4(c), no substantial differences can be observed between the two cases, neither

in the stroboscopic map nor in the histograms, except the fluctuations around the KAM torus location mentioned above. This behavior might be explained by the fact that the system automatically chooses an excitation frequency from the noise spectrum. This means that narrow-band noise is able to recover the intrinsic dynamics of the system, which can be also induced by an external periodic force. In the case of wide-band noise (δ is large enough), this effect will be hidden due to the interplay of other frequencies in the noise spectrum and the nonlinearity of the system. It is worth noticing that the large fluctuations around the KAM torus location, seen in Fig. 5(b), disappear if we further decrease δ . It seems that these fluctuations take place when the KAM tori are about to form, but disappear when they are already present in the stroboscopic map. In this sense, these fluctuations could be seen as a sign of KAM tori formation. These fluctuations near the KAM torus should be considered only as a qualitative difference between the deterministic and the stochastic cases, and it could not be considered as a quantitative measure.

Finally, we consider how the behavior of the system is modified when the central frequency of the harmonic noise ω_0 changes. For this purpose we have performed some numerical computations having fixed $\delta = 0.03$ and $\Delta = 0.001$, whereas ω_0 has been changed from $\omega_0 = \pi$ to $\omega_0 = 10\pi$ and $\omega_0 = 100\pi$. The result in this case is that the stroboscopic map is very similar to the pure deterministic one when ψ_{01} is time-independent, that is, $\mu = 0$ in Eq. (3). This fact can be considered as a stronger argument in favor of the explanation that the system itself chooses an excitation frequency from the noise spectrum. However, in this case, this excitation frequency does not carry any energy, because it is far away from the peak frequency of the harmonic noise. This means, that despite the noise excitation, an effective action of the noise on the flow model appears to be zero.

In conclusion, we have considered the influence of harmonic noise on the chaotic advection of fluid flow for different bandwidths of the noise. The main result obtained here is that the stochastic system can excite a behavior which resembles very closely that of the pure deterministic situation. This fact shows that the dynamics is mainly controlled by intrinsic properties of the system rather than by external factors. The fluctuations in the probability

distribution of noisy excitations around the KAM tori location are a phenomenon associated with the generation of the KAM tori under the influence of noise.

Acknowledgements

We acknowledge financial support from The Max-Planck-Gesellschaft (A.Z.), the Spanish Ministry of Science and Technology under project BFM2000-0967 and Acción Integrada Hispano-Alemana under project HA2000-0018 (J.P.B. and M.A.F.S.) and from the Deutsche Forschungsgemeinschaft (SFB 555) (J.K.).

References

- [1] R. Benzi, A. Sutera, A. Vulpiani, *J. Phys. A* 14 (1981) L453.
- [2] L. Gammaitoni, P. Hänggi, P. Jung, F. Marchesoni, *Rev. Mod. Phys.* 70 (1998) 223.
- [3] W. Horsthemke, R. Lefever, *Noise-Induced Transitions*, Springer, Berlin, 1984.
- [4] J. García-Ojalvo, J.M. Sancho, *Noise in Spatially Extended Systems*, Springer, New York, 1999.
- [5] P. Landa, A. Zaikin, *Phys. Rev. E* 54 (1996) 3535; P. Landa, A. Zaikin, V.G. Ushakov, J. Kurths, *Phys. Rev. E* 61 (2000) 4809.
- [6] F. Marchesoni, *Phys. Lett. A* 237 (1998) 126.
- [7] A. Pikovsky, J. Kurths, *Phys. Rev. Lett.* 78 (1997) 775.
- [8] J.M.R. Parrondo, C. Van der Broeck, J. Buceta, F.J. de la Rubia, *Physica A* 224 (1996) 153.
- [9] P. Landa, A. Rabinovitch, *Phys. Rev. E* 61 (2000) 1829.
- [10] P. Landa, *Europhys. Lett.* 36 (1996) 401.
- [11] H. Aref, *J. Fluid Mech.* 143 (1984) 1.
- [12] J.M. Ottino, *The Theory of Mixing: Stretching, Chaos and Transport*, Cambridge University Press, Cambridge, 1989.
- [13] R. Braun, Ph.D. Thesis, University of Potsdam, 1997.
- [14] A. Witt, R. Braun, F. Feudel, C. Grebogi, J. Kurths, *Phys. Rev. E* 59 (1999) 1605.
- [15] P. Tabeling, B. Perrin, S. Fauve, *Europhys. Lett.* 3 (1987) 459.
- [16] P. Tabeling, O. Cardoso, B. Perrin, *J. Fluid Mech.* 213 (1990) 511.
- [17] O. Cardoso, H. Willaime, P. Tabeling, *Phys. Rev. Lett.* 65 (1990) 1869.
- [18] H. Willaime, O. Cardoso, P. Tabeling, *Phys. Rev. E* 48 (1993) 288.
- [19] J.M. Finn, J.F. Drake, P.N. Guzdar, *Phys. Fluids B* 4 (1992) 2758.
- [20] P.N. Guzdar, J.M. Finn, A.V. Rogalsky, J.F. Drake, *Phys. Rev. E* 49 (1994) 2062.
- [21] R. Braun, F. Feudel, P.N. Guzdar, *Phys. Rev. E* 58 (1998) 1927.